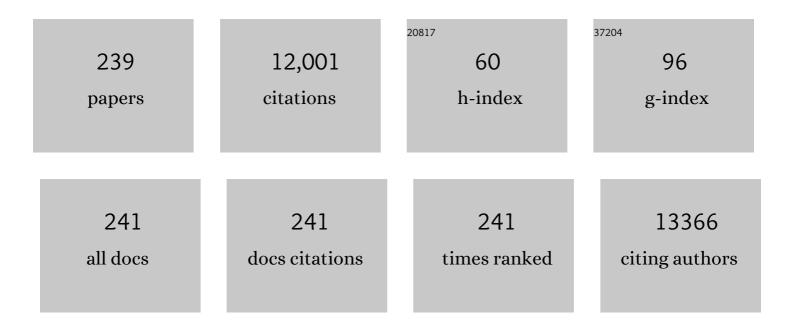
Qingzhong Xue

List of Publications by Year in descending order

Source: https://exaly.com/author-pdf/3771488/publications.pdf Version: 2024-02-01



#	Article	IF	CITATIONS
1	Polycyclic Aromatic Hydrocarbons as a New Class of Promising Cathode Materials for Aluminumâ€lon Batteries. Angewandte Chemie - International Edition, 2022, 61, e202114681.	13.8	37
2	Plate-barrier architecture of rGO-TiO2 derived from MXene for constructing well-aligned polymer nanocomposites with excellent dielectric performance. Composites Science and Technology, 2022, 218, 109191.	7.8	9
3	The miscible behaviors of C3H8/C8H18(C7H17N) system in nanoslits: Effects of pore size and rock surface wettability. Chemical Engineering Journal, 2022, 431, 133988.	12.7	2
4	A tin oxide/silicon heterojunction with a nano litchi shell structure for ultrafast, high-detectivity, self-powered broadband photodetectors. Journal of Materials Chemistry C, 2022, 10, 2049-2059.	5.5	8
5	Self-powered multifunctional monitoring and analysis system based on dual-triboelectric nanogenerator and chitosan/activated carbon film humidity sensor. Nano Energy, 2022, 94, 106881.	16.0	58
6	Sensing mechanism of acetone adsorption on charged ZnO and ZnSe surfaces: Insights from DFT calculations. Materials Today Communications, 2022, 31, 103238.	1.9	7
7	Sixâ€erm Stellat Dendriticâ€PbS Flexible Infrared Photodetector for Intelligent Healthcare Monitoring. Advanced Materials Technologies, 2022, 7, .	5.8	18
8	Multifunctional superwetting positively charged foams for continuous oil/water emulsion separation and removal of hazardous pollutants from water. Separation and Purification Technology, 2022, 289, 120683.	7.9	19
9	The effect of gas injection velocity and pore morphology on displacement mechanisms in porous media based on CFD approach. Journal of Natural Gas Science and Engineering, 2022, 101, 104558.	4.4	8
10	Trace nitrogen-incorporation stimulates dual active sites of nickel catalysts for efficient hydrogen oxidation electrocatalysis. Chemical Engineering Journal, 2022, 445, 136700.	12.7	11
11	Dual carbon Li-ion capacitor with high energy density and ultralong cycling life at a wide voltage window. Science China Materials, 2022, 65, 2373-2384.	6.3	5
12	Robust modified nylon mesh for the separation of crude-oil/water emulsion based on the coupling of squeezing coalescence demulsification and sieving separation. Separation and Purification Technology, 2022, 295, 121319.	7.9	9
13	DFT insights into the selective NH ₃ sensing mechanism of two dimensional ZnTe monolayer. Journal of Physics Condensed Matter, 2022, 34, 374002.	1.8	0
14	Dual-functional membrane decorated with flower-like metal–organic frameworks for highly efficient removal of insoluble emulsified oils and soluble dyes. Journal of Hazardous Materials, 2021, 408, 124444.	12.4	92
15	Dynamics and miscible behaviors of hydrocarbon gas and crude oil in nanoslits: Effects of light gas type and crude oil components. Chemical Engineering Journal, 2021, 405, 127012.	12.7	25
16	High-performance aluminum-polyaniline battery based on the interaction between aluminum ion and -NH groups. Science China Materials, 2021, 64, 318-328.	6.3	31
17	3D radial Co3O4 nanorod cluster derived from cobalt-based layered hydroxide metal salt for enhanced trace acetone detection. Sensors and Actuators B: Chemical, 2021, 327, 128926.	7.8	36
18	Multifunctional charged hydrogel nanofibrous membranes for metal ions contained emulsified oily wastewater purification. Journal of Membrane Science, 2021, 621, 118950.	8.2	45

#	Article	IF	CITATIONS
19	Ni-doped brochantite@copper hydroxide hierarchical structures on copper mesh with ultrahigh oil-resistance for high-efficiency oil/water separation. Surface and Coatings Technology, 2021, 406, 126642.	4.8	13
20	CH4 and CO2 Adsorption Mechanism in Kaolinite Slit Nanopores as Studied by the Grand Canonical Monte Carlo Method. Journal of Nanoscience and Nanotechnology, 2021, 21, 108-119.	0.9	2
21	Improving the performance of lithium ion capacitor by stabilizing anode working potential using CoSe2 nanoparticles embedded nitrogen-doped hard carbon microspheres. Electrochimica Acta, 2021, 370, 137717.	5.2	17
22	ZIF-8 derived ZnO polyhedrons decorated with biomass derived nitrogen-doped porous carbon for enhanced acetone sensing. Sensors and Actuators B: Chemical, 2021, 330, 129366.	7.8	46
23	Critical factors controlling adsorption capacity of shale gas in Wufeng-Longmaxi formation, Sichuan Basin: Evidences from both experiments and molecular simulations. Journal of Natural Gas Science and Engineering, 2021, 88, 103774.	4.4	24
24	Waterâ€Soluble Salt Templateâ€Assisted Anchor of Hollow FeS ₂ Nanoparticle Inside 3D Carbon Skeleton to Achieve Fast Potassiumâ€Ion Storage. Advanced Energy Materials, 2021, 11, 2101343.	19.5	56
25	Enhancing oil-in-water emulsion separation performance of polyvinyl alcohol hydrogel nanofibrous membrane by squeezing coalescence demulsification. Journal of Membrane Science, 2021, 630, 119324.	8.2	61
26	Stimulation of surface terminating group by carbon quantum dots for improving pseudocapacitance of Ti3C2Tx MXene based electrode. Carbon, 2021, 180, 118-126.	10.3	32
27	Reusable membrane with multifunctional skin layer for effective removal of insoluble emulsified oils and soluble dyes. Journal of Hazardous Materials, 2021, 415, 125677.	12.4	86
28	Hierarchical superhydrophobic polydimethylsiloxane/copper terephthalate/polyurethane sponge for highly efficient oil/water separation. Colloids and Surfaces A: Physicochemical and Engineering Aspects, 2021, 630, 127635.	4.7	24
29	Amorphous Se species anchored into enclosed carbon skeleton bridged by chemical bonding toward advanced K-Se batteries. Journal of Energy Chemistry, 2021, 61, 319-326.	12.9	15
30	Bimetallic metal–organic frameworks derived hierarchical flower-like Zn-doped Co3O4 for enhanced acetone sensing properties. Applied Surface Science, 2021, 565, 150520.	6.1	26
31	The miscible behaviors and mechanism of CO2/CH4/C3H8/N2 and crude oil in nanoslits: A molecular dynamics simulation study. Fuel, 2021, 304, 121461.	6.4	26
32	Molecular insights into carbon dioxide enhanced multi-component shale gas recovery and its sequestration in realistic kerogen. Chemical Engineering Journal, 2021, 425, 130292.	12.7	49
33	End Group Modification for Black Phosphorus: Simultaneous Improvement of Chemical Stability and Gas Sensing Performance. ACS Applied Materials & Interfaces, 2021, 13, 50270-50280.	8.0	16
34	Embedded SnO2/Diatomaceous earth composites for fast humidity sensing and controlling properties. Sensors and Actuators B: Chemical, 2020, 303, 127137.	7.8	22
35	Graphitic carbon nitride catalyzes selective oxidative dehydrogenation of propane. Applied Catalysis B: Environmental, 2020, 262, 118277.	20.2	47
36	Doping-induced enhancement of CO2 adsorption on negatively charged C3N nanosheet: Insights from DFT calculations. Chemical Engineering Journal, 2020, 387, 123403.	12.7	21

#	Article	IF	CITATIONS
37	Metal-organic frameworks derived ZnO@MoS nanosheets core/shell heterojunctions for ppb-level acetone detection: Ultra-fast response and recovery. Sensors and Actuators B: Chemical, 2020, 304, 127430.	7.8	57
38	Small graphite nanoflakes as an advanced cathode material for aluminum ion batteries. Chemical Communications, 2020, 56, 1593-1596.	4.1	24
39	Metal-organic frameworks derived hierarchical flower-like ZnO/ Co3O4 heterojunctions for ppb-level acetone detection. Sensors and Actuators B: Chemical, 2020, 325, 128814.	7.8	52
40	High performance aluminum ion battery using polyaniline/ordered mesoporous carbon composite. Journal of Power Sources, 2020, 477, 228702.	7.8	33
41	Flexible SnSe Photodetectors with Ultrabroad Spectral Response up to 10.6 μm Enabled by Photobolometric Effect. ACS Applied Materials & Interfaces, 2020, 12, 35250-35258.	8.0	73
42	Great Enhancement of Selfâ€Powered Photoresponse Performance of C ₃ H ₈ NSiâ€TiO ₂ NRAs/nâ€Si Heterojunction by Buildâ€In and Buildâ€Out Electric Field Jointly Promoting Carrier Separation. Advanced Electronic Materials, 2020, 6, 2000501.	5.1	10
43	Theoretical study of strain-controlled C2X (XÂ=ÂN, O) membrane for CO2/C2H2 separation. Applied Surface Science, 2020, 530, 147250.	6.1	7
44	Surface lattice reconstruction enhanced the photoresponse performance of a self-powered ZnO nanorod arrays/Si heterojunction photodetector. Journal of Materials Chemistry C, 2020, 8, 17440-17449.	5.5	13
45	Adsorption and absorption of supercritical methane within shale kerogen slit. Journal of Molecular Liquids, 2020, 320, 114364.	4.9	23
46	β-Hydrogen of Polythiophene Induced Aluminum Ion Storage for High-Performance Al-Polythiophene Batteries. ACS Applied Materials & Interfaces, 2020, 12, 46065-46072.	8.0	31
47	Bioinspired Anti-Oil-Fouling Hierarchical Structured Membranes Decorated with Urchin-Like α-FeOOH Particles for Efficient Oil/Water Mixture and Crude Oil-in-Water Emulsion Separation. ACS Applied Materials & Interfaces, 2020, 12, 50962-50970.	8.0	40
48	UV assisted ppb-level acetone detection based on hollow ZnO/MoS2 nanosheets core/shell heterostructures at low temperature. Sensors and Actuators B: Chemical, 2020, 317, 128208.	7.8	74
49	Enhanced gas separation performance of Pebax mixed matrix membranes by incorporating ZIF-8 in situ inserted by multiwalled carbon nanotubes. Separation and Purification Technology, 2020, 248, 117080.	7.9	49
50	Wafer-size growth of 2D layered SnSe films for UV-Visible-NIR photodetector arrays with high responsitivity. Nanoscale, 2020, 12, 7358-7365.	5.6	53
51	Folding 2D Graphene Nanoribbons into 3D Nanocages Induced by Platinum Nanoclusters. Journal of Physical Chemistry C, 2020, 124, 10495-10501.	3.1	4
52	The miscible behaviors of C10H22(C7H17N)/C3H8 system: Insights from molecular dynamics simulations. Fuel, 2020, 279, 118445.	6.4	19
53	SnO2 nanoparticles-modified 3D-multilayer MoS2 nanosheets for ammonia gas sensing at room temperature. Sensors and Actuators B: Chemical, 2020, 321, 128471.	7.8	71
54	High-performance aqueous sodium-ion battery using a hybrid electrolyte with a wide electrochemical stability window. RSC Advances, 2020, 10, 25496-25499.	3.6	16

#	Article	IF	CITATIONS
55	Autonomous Drug Release Systems with Disease Symptomâ€Associated Triggers. Advanced Intelligent Systems, 2020, 2, 1900124.	6.1	14
56	Microphone-like Cu-CAT-1 hierarchical structures with ultra-low oil adhesion for highly efficient oil/water separation. Separation and Purification Technology, 2020, 241, 116688.	7.9	24
57	Enhanced energy storage density and discharge efficiency in potassium sodium niobite-based ceramics prepared using a new scheme. Journal of the European Ceramic Society, 2020, 40, 2357-2365.	5.7	41
58	Layered double hydroxides derived NiCo-sulfide as a cathode material for aluminum ion batteries. Electrochimica Acta, 2020, 344, 136174.	5.2	26
59	One-step synthesis of a robust and anti-oil-fouling biomimetic cactus-like hierarchical architecture for highly efficient oil/water separation. Environmental Science: Nano, 2020, 7, 903-911.	4.3	28
60	Review—Open-Framework Structure Based Cathode Materials Coupled with Metallic Anodes for Rechargeable Multivalent Ion Batteries. Journal of the Electrochemical Society, 2020, 167, 160530.	2.9	4
61	Lattice Boltzmann method for simulation of shale gas flow in kerogen nano-pores considering temperature dependent adsorption. International Journal of Oil, Gas and Coal Technology, 2020, 23, 409.	0.2	0
62	Flexible self-powered high-performance ammonia sensor based on Au-decorated MoSe2 nanoflowers driven by single layer MoS2-flake piezoelectric nanogenerator. Nano Energy, 2019, 65, 103974.	16.0	281
63	TiO ₂ @TiO _{2â~'x} Hx core-shell nanoparticle film/Si heterojunction for ultrahigh detectivity and sensitivity broadband photodetector. Nanotechnology, 2019, 30, 415203.	2.6	4
64	Co-MOF-74 derived Co3O4/graphene heterojunction nanoscrolls for ppb-level acetone detection. Sensors and Actuators B: Chemical, 2019, 300, 127011.	7.8	62
65	Solution quenched in-situ growth of hierarchical flower-like NiFe2O4/Fe2O3 heterojunction for wide-range light absorption. Journal of Power Sources, 2019, 440, 227120.	7.8	20
66	Charge-controlled switchable H2 storage on conductive borophene nanosheet. International Journal of Hydrogen Energy, 2019, 44, 20150-20157.	7.1	26
67	Investigation of pore size effects on adsorption behavior of shale gas. Marine and Petroleum Geology, 2019, 109, 1-8.	3.3	45
68	Oxygen vacancies enhanced photoresponsive performance of ZnO nanoparticles thin film/Si heterojunctions for ultraviolet/infrared photodetector. Journal of Alloys and Compounds, 2019, 797, 1224-1231.	5.5	26
69	Revealing the impacting factors of cathodic carbon catalysts for Li-CO2 batteries in the pore-structure point of view. Electrochimica Acta, 2019, 311, 41-49.	5.2	28
70	A ZIF-8@H:ZnO core–shell nanorod arrays/Si heterojunction self-powered photodetector with ultrahigh performance. Journal of Materials Chemistry C, 2019, 7, 5172-5183.	5.5	15
71	A hierarchical structured steel mesh decorated with metal organic framework/graphene oxide for high-efficient oil/water separation. Journal of Hazardous Materials, 2019, 373, 725-732.	12.4	120
72	A durable mesh decorated with polydopamine/graphene oxide for highly efficient oil/water mixture separation. Applied Surface Science, 2019, 479, 351-359.	6.1	51

#	Article	IF	CITATIONS
73	High-efficiency separation performance of oil-water emulsions of polyacrylonitrile nanofibrous membrane decorated with metal-organic frameworks. Applied Surface Science, 2019, 476, 61-69.	6.1	103
74	Layer-by-layer self-assembly of polyaniline nanofibers/TiO ₂ nanotubes heterojunction thin film for ammonia detection at room temperature. Nanotechnology, 2019, 30, 135501.	2.6	20
75	Critical factors controlling shale gas adsorption mechanisms on Different Minerals Investigated Using GCMC simulations. Marine and Petroleum Geology, 2019, 100, 31-42.	3.3	22
76	Confined hetero double helix structure induced by graphene nanoribbon. 2D Materials, 2019, 6, 034001.	4.4	5
77	Numerical simulation of enhancing shale gas recovery using electrical resistance heating method. International Journal of Heat and Mass Transfer, 2019, 128, 1218-1228.	4.8	14
78	Multi-shelled ZnCo2O4 yolk-shell spheres for high-performance acetone gas sensor. Applied Surface Science, 2018, 443, 114-121.	6.1	77
79	Synthesis of nanowire bundle-like WO3-W18O49 heterostructures for highly sensitive NH3 sensor application. Journal of Hazardous Materials, 2018, 353, 290-299.	12.4	94
80	Ultrahigh photosensitivity and detectivity of hydrogen-treated TiO ₂ nanorod array/SiO ₂ /Si heterojunction broadband photodetectors and its mechanism. Journal of Materials Chemistry C, 2018, 6, 2319-2328.	5.5	21
81	Charge-modulated CO2 capture of C3N nanosheet: Insights from DFT calculations. Chemical Engineering Journal, 2018, 338, 92-98.	12.7	111
82	GCMC simulations on the adsorption mechanisms of CH4 and CO2 in K-illite and their implications for shale gas exploration and development. Fuel, 2018, 224, 521-528.	6.4	55
83	S-graphite slit pore: A superior selective adsorbent for light hydrocarbons. Applied Surface Science, 2018, 444, 772-779.	6.1	18
84	Ultra-sensitive NH3 sensor based on flower-shaped SnS2 nanostructures with sub-ppm detection ability. Journal of Hazardous Materials, 2018, 341, 159-167.	12.4	140
85	Outstanding capacitive performance of ordered mesoporous carbon modified by anthraquinone. Electrochimica Acta, 2018, 259, 110-121.	5.2	37
86	Inherent wettability of different rock surfaces at nanoscale: a theoretical study. Applied Surface Science, 2018, 434, 73-81.	6.1	51
87	Chemically functionalized 3D reticular graphene oxide frameworks decorated with MOF-derived Co3O4: Towards highly sensitive and selective detection to acetone. Sensors and Actuators B: Chemical, 2018, 259, 289-298.	7.8	73
88	Carbon-encapsulated CoSe nanoparticles derived from metal-organic frameworks as advanced cathode material for Al-ion battery. Journal of Power Sources, 2018, 401, 6-12.	7.8	94
89	Me–N–C (Me = Fe, Cu, and Co) nanosheet as a promising charge-controlled CO2 capture material. Journal of Materials Chemistry A, 2018, 6, 12404-12410.	10.3	27
90	High-performance WO _{3â^'x} -WSe ₂ /SiO ₂ /n-Si heterojunction near-infrared photodetector <i>via</i> a homo-doping strategy. Journal of Materials Chemistry C, 2018, 6, 5821-5829.	5.5	34

#	Article	IF	CITATIONS
91	Stable CoSe ₂ /carbon nanodice@reduced graphene oxide composites for high-performance rechargeable aluminum-ion batteries. Energy and Environmental Science, 2018, 11, 2341-2347.	30.8	240
92	Great enhancement of CH4 sensitivity of SnO2 based nanofibers by heterogeneous sensitization and catalytic effect. Sensors and Actuators B: Chemical, 2018, 254, 393-401.	7.8	65
93	Ultra-high selective capture of CO 2 on one-sided N-doped carbon nanoscrolls. Journal of CO2 Utilization, 2017, 18, 275-282.	6.8	22
94	Effects of Sulfur Doping and Humidity on CO ₂ Capture by Graphite Split Pore: A Theoretical Study. ACS Applied Materials & Interfaces, 2017, 9, 8336-8343.	8.0	53
95	Keys to linking GCMC simulations and shale gas adsorption experiments. Fuel, 2017, 199, 14-21.	6.4	84
96	Defective germanene as a high-efficiency helium separation membrane: a first-principles study. Nanotechnology, 2017, 28, 135703.	2.6	12
97	Functionalization of petroleum coke-based mesoporous carbon for synergistically enhanced capacitive performance. Journal of Materials Research, 2017, 32, 1248-1257.	2.6	7
98	Enhanced Room Temperature Oxygen Sensing Properties of LaOCl–SnO ₂ Hollow Spheres by UV Light Illumination. ACS Sensors, 2017, 2, 679-686.	7.8	43
99	Theoretical study of H 2 separation performance of two-dimensional graphitic carbon oxide membrane. International Journal of Hydrogen Energy, 2017, 42, 13120-13126.	7.1	17
100	Mixed Matrix Membranes with Excellent CO ₂ Capture Induced by Nano arbon Hybrids. ChemNanoMat, 2017, 3, 560-568.	2.8	12
101	Ultrahigh broadband photoresponse of SnO ₂ nanoparticle thin film/SiO ₂ /p-Si heterojunction. Nanoscale, 2017, 9, 8848-8857.	5.6	41
102	Ultrahigh permittivity of polymer nanocomposites based on surface-modified amorphous carbon/MWCNTs shell/core structured nanohybrids. Composites Part A: Applied Science and Manufacturing, 2017, 100, 324-332.	7.6	9
103	Remarkable supercapacitor performance of petal-like LDHs vertically grown on graphene/polypyrrole nanoflakes. Journal of Materials Chemistry A, 2017, 5, 8964-8971.	10.3	53
104	Antifouling hydrolyzed polyacrylonitrile/graphene oxide membrane with spindle-knotted structure for highly effective separation of oil-water emulsion. Journal of Membrane Science, 2017, 532, 38-46.	8.2	170
105	Effective enhancement of gas separation performance in mixed matrix membranes using core/shell structured multi-walled carbon nanotube/graphene oxide nanoribbons. Nanotechnology, 2017, 28, 065702.	2.6	40
106	Pinning Down the Anomalous Light Soaking Effect toward High-Performance and Fast-Response Perovskite Solar Cells: The Ion-Migration-Induced Charge Accumulation. Journal of Physical Chemistry Letters, 2017, 8, 5069-5076.	4.6	60
107	Superior Selective CO ₂ Adsorption of C ₃ N Pores: GCMC and DFT Simulations. ACS Applied Materials & amp; Interfaces, 2017, 9, 31161-31169.	8.0	79
108	Insight of synergistic effect of different active metal ions in layered double hydroxides on their electrochemical behaviors. Electrochimica Acta, 2017, 253, 302-310.	5.2	67

#	Article	IF	CITATIONS
109	Fluorine-rich carbon nanoscrolls for CO2/CO (C2H2) adsorptive separation. Journal of CO2 Utilization, 2017, 21, 429-435.	6.8	12
110	Electrostatic Self-Assembly of Sandwich-Like CoAl-LDH/Polypyrrole/Graphene Nanocomposites with Enhanced Capacitive Performance. ACS Applied Materials & amp; Interfaces, 2017, 9, 31699-31709.	8.0	103
111	585 divacancy-defective germanene as a hydrogen separation membrane: A DFT study. International Journal of Hydrogen Energy, 2017, 42, 24189-24196.	7.1	33
112	Facile synthesis of La 2 O 2 CO 3 nanoparticle films and Its CO 2 sensing properties and mechanisms. Applied Surface Science, 2017, 426, 725-733.	6.1	36
113	Bifuntional petaloid nickel manganese layered double hydroxides decorated on a freestanding carbon foam for flexible asymmetric supercapacitor and oxygen evolution. Electrochimica Acta, 2017, 252, 275-285.	5.2	30
114	Extracting the inner wall from nested double-walled carbon nanotube by platinum nanowire: molecular dynamics simulations. RSC Advances, 2017, 7, 39480-39489.	3.6	6
115	Pore-scale characterization of tight sandstone in Yanchang Formation Ordos Basin China using micro-CT and SEM imaging from nm- to cm-scale. Fuel, 2017, 209, 254-264.	6.4	107
116	Sulfur–Nitrogen Codoped Graphite Slit-Pore for Enhancing Selective Carbon Dioxide Adsorption: Insights from Molecular Simulations. ACS Sustainable Chemistry and Engineering, 2017, 5, 8815-8823.	6.7	23
117	Two-dimensional graphene oxide membrane for H2/CH4 separation: Insights from molecular dynamics simulations. International Journal of Hydrogen Energy, 2017, 42, 30653-30660.	7.1	28
118	Effect of the Wettability on Two-Phase Flow Inside Porous Medium at Nanoscale: Lattice Boltzmann Simulations. Journal of Nanoscience and Nanotechnology, 2017, 17, 6620-6625.	0.9	1
119	ZIF-derived porous ZnO-Co3O4 hollow polyhedrons heterostructure with highly enhanced ethanol detection performance. Sensors and Actuators B: Chemical, 2017, 253, 523-532.	7.8	108
120	Layered double hydroxides toward high-performance supercapacitors. Journal of Materials Chemistry A, 2017, 5, 15460-15485.	10.3	326
121	Effective CO2 detection based on LaOCl-doped SnO2 nanofibers: Insight into the role of oxygen in carrier gas. Sensors and Actuators B: Chemical, 2017, 241, 725-734.	7.8	69
122	Graphene oxide/polyacrylonitrile fiber hierarchical-structured membrane for ultra-fast microfiltration of oil-water emulsion. Chemical Engineering Journal, 2017, 307, 643-649.	12.7	303
123	Molecular Simulation of Oil Mixture Adsorption Character in Shale System. Journal of Nanoscience and Nanotechnology, 2017, 17, 6198-6209.	0.9	15
124	Quantitative Characterization of the Effect of Interfacial Fluid Layer on Water Flow Inside Nano-Porous Medium Using the Lattice Boltzmann Method. Journal of Nanoscience and Nanotechnology, 2017, 17, 6216-6223.	0.9	1
125	Effective Enhancement of Humidity Sensing Characteristics of Novel Thermally Treated MWCNTs/Polyvinylpyrrolidone Film Caused by Interfacial Effect. Advanced Materials Interfaces, 2016, 3, 1600153.	3.7	10
126	Hierarchical NiO Nanoflake Arrays on Nickel Foam as a Supercapacitor Electrode with High Capacitance and High Rate Capability. Journal of Nanoscience and Nanotechnology, 2016, 16, 4169-4173.	0.9	1

#	Article	IF	CITATIONS
127	Excellent dielectric properties of PVDF-based composites filled with carbonized PAN/PEG copolymer fibers. Composites Part A: Applied Science and Manufacturing, 2016, 87, 46-53.	7.6	25
128	Sandwich-like graphene/polypyrrole/layered double hydroxide nanowires for high-performance supercapacitors. Journal of Power Sources, 2016, 331, 67-75.	7.8	62
129	Theoretical study of a tunable and strain-controlled nanoporous graphenylene membrane for multifunctional gas separation. Journal of Materials Chemistry A, 2016, 4, 15015-15021.	10.3	65
130	Self-Assembly of Hydrofluorinated Janus Graphene Monolayer: A Versatile Route for Designing Novel Janus Nanoscrolls. Scientific Reports, 2016, 6, 26914.	3.3	18
131	Super flexibility and stability of graphene nanoribbons under severe twist. Physical Chemistry Chemical Physics, 2016, 18, 18406-18413.	2.8	21
132	High hydrogen sensitivity of vertically standing layered MoS2/Si heterojunctions. Journal of Alloys and Compounds, 2016, 682, 29-34.	5.5	36
133	Understanding the relationship between ion migration and the anomalous hysteresis in high-efficiency perovskite solar cells: A fresh perspective from halide substitution. Nano Energy, 2016, 26, 620-630.	16.0	167
134	Ultraâ€high dielectric constant of poly(vinylidene fluoride) composites filled with hydroxyl modified graphite powders. Polymer Composites, 2016, 37, 327-333.	4.6	7
135	Room temperature hydrogen sensor with ultrahigh-responsive characteristics based on Pd/SnO2/SiO2/Si heterojunctions. Sensors and Actuators B: Chemical, 2016, 227, 438-447.	7.8	39
136	Self-powered broadband, high-detectivity and ultrafast photodetectors based on Pd-MoS ₂ /Si heterojunctions. Physical Chemistry Chemical Physics, 2016, 18, 1131-1139.	2.8	44
137	Sandwich-like nitrogen-doped porous carbon/graphene nanoflakes with high-rate capacitive performance. Nanoscale, 2016, 8, 7889-7898.	5.6	54
138	How to select an optimal surfactant molecule to speed up the oil-detachment from solid surface: A computational simulation. Chemical Engineering Science, 2016, 147, 47-53.	3.8	42
139	Effect of interfacial layer on water flow in nanochannels: Lattice Boltzmann simulations. Physica B: Condensed Matter, 2016, 487, 18-24.	2.7	11
140	Outstanding capacitive performance of reticular porous carbon/graphene sheets with superhigh surface area. Electrochimica Acta, 2016, 190, 923-931.	5.2	32
141	Helical wrapping of long-chained polyacetylene (PA) on metallic nanowires: MD simulation insights. Computational Materials Science, 2016, 117, 103-109.	3.0	5
142	Ultrafast breathing humidity sensing properties of low-dimensional Fe-doped SnO ₂ flower-like spheres. RSC Advances, 2016, 6, 27008-27015.	3.6	30
143	Preparation of spherical and dendritic CdS@TiO2 hollow double-shelled nanoparticles for photocatalysis. Materials Letters, 2016, 166, 113-115.	2.6	21
144	Enhanced photovoltaic characteristics of MoS ₂ /Si hybrid solar cells by metal Pd chemical doping. RSC Advances, 2016, 6, 1346-1350.	3.6	14

#	Article	IF	CITATIONS
145	Fabrication and characterization of an ultrasensitive humidity sensor based on metal oxide/graphene hybrid nanocomposite. Sensors and Actuators B: Chemical, 2016, 225, 233-240.	7.8	367
146	Extraction of kerogen from oil shale with supercritical carbon dioxide: Molecular dynamics simulations. Journal of Supercritical Fluids, 2016, 107, 499-506.	3.2	58
147	Theoretical Prediction of Hydrogen Separation Performance of Two-Dimensional Carbon Network of Fused Pentagon. ACS Applied Materials & Interfaces, 2015, 7, 28502-28507.	8.0	36
148	Superhigh-rate capacitive performance of heteroatoms-doped double shell hollow carbon spheres. Carbon, 2015, 86, 235-244.	10.3	68
149	Electrical characterization and ammonia sensing properties of MoS2/Si p–n junction. Journal of Alloys and Compounds, 2015, 631, 105-110.	5.5	46
150	Gigantic enhancement in the dielectric properties of polymer-based composites using core/shell MWCNT/amorphous carbon nanohybrids. Nanoscale, 2015, 7, 3660-3667.	5.6	78
151	Mechanism of oil molecules transportation in nano-sized shale channel: MD simulation. RSC Advances, 2015, 5, 25684-25692.	3.6	28
152	High performance sponge MnO ₂ nanotube monoliths. RSC Advances, 2015, 5, 60831-60834.	3.6	4
153	Oil detachment from silica surface modified by carboxy groups in aqueous cetyltriethylammonium bromide solution. Applied Surface Science, 2015, 353, 1103-1111.	6.1	36
154	High-performance n-MoS ₂ /i-SiO ₂ /p-Si heterojunction solar cells. Nanoscale, 2015, 7, 8304-8308.	5.6	99
155	Electrical and photovoltaic characteristics of MoS2/Si <i>p-n</i> junctions. Journal of Applied Physics, 2015, 117, .	2.5	131
156	Growth and humidity-dependent electrical properties of bulk-like MoS ₂ thin films on Si. RSC Advances, 2015, 5, 74329-74335.	3.6	27
157	Insight into high areal capacitances of low apparent surface area carbons derived from nitrogen-rich polymers. Carbon, 2015, 94, 560-567.	10.3	56
158	C ₂ N: an excellent two-dimensional monolayer membrane for He separation. Journal of Materials Chemistry A, 2015, 3, 21351-21356.	10.3	157
159	Iron-doping-enhanced photoelectrochemical water splitting performance of nanostructured WO ₃ : a combined experimental and theoretical study. Nanoscale, 2015, 7, 2933-2940.	5.6	171
160	Carbon nanoscroll from C ₄ H/C ₄ F-type graphene superlattice: MD and MM simulation insights. Physical Chemistry Chemical Physics, 2015, 17, 3441-3450.	2.8	12
161	Photoelectrochemical Properties of Alkali Metal Doped TiO ₂ Nano-Honeycomb Film. Energy and Environment Focus, 2015, 4, 191-195.	0.3	2
162	Electric Field Manipulated CO ₂ Capture and Sequestration of Calcium-Graphene. Science of Advanced Materials, 2015, 7, 239-248.	0.7	8

#	Article	IF	CITATIONS
163	Excellent dielectric properties of Polyvinylidene fluoride composites based on sandwich structured MnO2/graphene nanosheets/MnO2. Composites Part A: Applied Science and Manufacturing, 2014, 67, 252-258.	7.6	47
164	Humidity sensitive properties of amorphous (K,Na)NbO3 lead free thin films. Ceramics International, 2014, 40, 10263-10267.	4.8	25
165	Superior capacitive performance of active carbons derived from Enteromorpha prolifera. Electrochimica Acta, 2014, 133, 459-466.	5.2	162
166	Preparation of large diameter and low density ZnS microtube arrays via a sacrificial template method. Materials Letters, 2014, 115, 140-143.	2.6	6
167	Studies in the capacitance properties of diaminoalkane-intercalated graphene. Electrochimica Acta, 2014, 148, 220-227.	5.2	6
168	Highly enhanced sensitivity of hydrogen sensors using novel palladium-decorated graphene nanoribbon film/SiO ₂ /Si structures. Journal of Materials Chemistry A, 2014, 2, 15931-15937.	10.3	31
169	Mechanical Properties of Hydrogenated Carbon Nanotubes (C ₄ HNTs): A Theoretical Study. Journal of Physical Chemistry C, 2014, 118, 16087-16094.	3.1	7
170	High hydrogen response of Pd/TiO2/SiO2/Si multilayers at room temperature. Sensors and Actuators B: Chemical, 2014, 205, 255-260.	7.8	25
171	Ultrahigh performance humidity sensor based on layer-by-layer self-assembly of graphene oxide/polyelectrolyte nanocomposite film. Sensors and Actuators B: Chemical, 2014, 203, 263-270.	7.8	242
172	Great enhancement in H2 response using graphene-based Schottky junction. Materials Letters, 2014, 135, 151-153.	2.6	15
173	On the origin of the high capacitance of carbon derived from seaweed with an apparently low surface area. Journal of Materials Chemistry A, 2014, 2, 18998-19004.	10.3	65
174	Fluorine-Modified Porous Graphene as Membrane for CO ₂ /N ₂ Separation: Molecular Dynamic and First-Principles Simulations. Journal of Physical Chemistry C, 2014, 118, 7369-7376.	3.1	114
175	The effect of oxygen molecule on the hydrogen storage process of Li-doped graphene. Chemical Physics Letters, 2014, 599, 100-103.	2.6	11
176	Tunable Hydrogen Separation in Porous Graphene Membrane: First-Principle and Molecular Dynamic Simulation. ACS Applied Materials & Interfaces, 2014, 6, 8048-8058.	8.0	159
177	Self-Assembly of Helical Polyacetylene Nanostructures on Carbon Nanotubes. Journal of Physical Chemistry C, 2013, 117, 16248-16255.	3.1	20
178	Structure control of ultra-large graphene oxide sheets by the Langmuir–Blodgett method. RSC Advances, 2013, 3, 4680.	3.6	36
179	Porous graphene sandwich/poly(vinylidene fluoride) composites with high dielectric properties. Composites Science and Technology, 2013, 86, 70-75.	7.8	79
180	Self-assembly of C4H-type hydrogenated graphene. Nanoscale, 2013, 5, 11132.	5.6	27

#	Article	IF	CITATIONS
181	Self-assembly of double helical nanostructures inside carbon nanotubes. Nanoscale, 2013, 5, 4191.	5.6	40
182	Hydrogen storage and release by bending carbon nanotubes. Computational Materials Science, 2013, 68, 121-126.	3.0	33
183	Hydrogen gas sensing properties of Pd/a-C:Pd/SiO2/Si structure at room temperature. Sensors and Actuators B: Chemical, 2013, 186, 796-801.	7.8	27
184	Critical role of small micropores in high CO2 uptake. Physical Chemistry Chemical Physics, 2013, 15, 2523.	2.8	228
185	Glass transition temperature of functionalized graphene–polymer composites. Computational Materials Science, 2013, 71, 66-71.	3.0	58
186	Carbon Doping of Hexagonal Boron Nitride by Using CO Molecules. Journal of Physical Chemistry C, 2013, 117, 9332-9339.	3.1	42
187	The preparation, load and photocatalytic performance of N-doped and CdS-coupled TiO2. RSC Advances, 2013, 3, 9483.	3.6	20
188	Effect of functional groups on the radial collapse and elasticity of carbon nanotubes under hydrostatic pressure. Nanoscale, 2012, 4, 3894.	5.6	14
189	Carbon/Silicon Heterojunction Formed by Inserting Carbon Nanotubes into Silicon Nanotubes: Molecular Dynamics Simulations. Journal of Physical Chemistry C, 2012, 116, 23181-23187.	3.1	4
190	High-rate capacitive performance of graphene aerogel with a superhigh C/O molar ratio. Journal of Materials Chemistry, 2012, 22, 23186.	6.7	145
191	Large photoconductivity of Pd doped amorphous carbon film/SiO2/Si. Diamond and Related Materials, 2012, 21, 24-27.	3.9	10
192	Influence of chemical functionalization on the CO2/N2 separation performance of porous graphene membranes. Nanoscale, 2012, 4, 5477.	5.6	193
193	Effect of chemisorption structure on the interfacial bonding characteristics of graphene–polymer composites. Applied Surface Science, 2012, 258, 2077-2082.	6.1	46
194	Diverse nanowires activated self-scrolling of graphene nanoribbons. Applied Surface Science, 2012, 258, 1964-1970.	6.1	20
195	Theoretical approaches to graphene and graphene-based materials. Nano Today, 2012, 7, 180-200.	11.9	122
196	Adsorption and Catalytic Activation of O ₂ Molecule on the Surface of Au-Doped Graphene under an External Electric Field. Journal of Physical Chemistry C, 2012, 116, 19918-19924.	3.1	99
197	Release of encapsulated molecules from carbon nanotubes using a displacing method: a MD simulation study. RSC Advances, 2012, 2, 6913.	3.6	20
198	Fabrication of carbon nanotube/graphene core/shell nanostructures on SiO2 substrates using organic solvents: A molecular dynamics study. Science Bulletin, 2012, 57, 3030-3035.	1.7	2

#	Article	IF	CITATIONS
199	Effect of defects on Young's modulus of graphene sheets: a molecular dynamics simulation. RSC Advances, 2012, 2, 9124.	3.6	142
200	Influence of substrate resistivity on photovoltaic characteristics of Pdâ€doped amorphous carbon film/SiO ₂ /Si heterojunction. Physica Status Solidi (A) Applications and Materials Science, 2012, 209, 1359-1362.	1.8	4
201	Fabrication of Carbon Nanoscrolls from Monolayer Graphene Controlled by P-Doped Silicon Nanowires: A MD Simulation Study. Journal of Physical Chemistry C, 2011, 115, 15217-15224.	3.1	37
202	Molecule Delivery by the Domino Effect of Carbon Nanotubes. Journal of Physical Chemistry C, 2011, 115, 20471-20480.	3.1	13
203	Influence of polarity on filling polymer molecules into carbon nanotubes. Computational Materials Science, 2011, 50, 2909-2917.	3.0	4
204	Effect of ethanol gas on the electrical properties of ZnO nanorods. Physica E: Low-Dimensional Systems and Nanostructures, 2011, 43, 1056-1060.	2.7	28
205	Influence of interfaces on impedance response and breakdown of oxide–metal multilayer structures. Thin Solid Films, 2011, 519, 3196-3202.	1.8	4
206	Effect of Si substrate on ethanol gas sensing properties of ZnO films. Thin Solid Films, 2011, 519, 6151-6154.	1.8	9
207	Current–voltage characteristics and ethanol gas sensing properties of ZnO thin film/Si heterojunction at room temperature. Physica E: Low-Dimensional Systems and Nanostructures, 2010, 42, 2021-2025.	2.7	32
208	Fabrication of Carbon Nanoscrolls from Monolayer Graphene. Small, 2010, 6, 2010-2019.	10.0	127
209	Effect of Chemisorption on the Interfacial Bonding Characteristics of Grapheneâ^'Polymer Composites. Journal of Physical Chemistry C, 2010, 114, 6588-6594.	3.1	150
210	Influence of Solid Surface and Functional Group on the Collapse of Carbon Nanotubes. Journal of Physical Chemistry C, 2010, 114, 2100-2107.	3.1	28
211	Different factors' effect on the SWNT-fluorocarbon resin interaction: A MD simulation study. Computational Materials Science, 2010, 49, 148-157.	3.0	22
212	Silicon/graphene core/shell nanowires produced by self-scrolling. Computational Materials Science, 2010, 49, 588-592.	3.0	22
213	Room-temperature high-sensitivity detection of ammonia gas using the capacitance of carbon/silicon heterojunctions. Energy and Environmental Science, 2010, 3, 288.	30.8	60
214	Investigation of the interactions between molecules of β-Carotene, Vitamin A and CNTs by MD simulations. Materials Letters, 2009, 63, 319-321.	2.6	12
215	Computational analysis of effect of modification on the interfacial characteristics of a carbon nanotube–polyethylene composite system. Applied Surface Science, 2009, 255, 3534-3543.	6.1	127
216	Radial Collapse of Single-Walled Carbon Nanotubes Induced by the Cu ₂ O Surface. Journal of Physical Chemistry C, 2009, 113, 3120-3126.	3.1	30

#	Article	IF	CITATIONS
217	Chemical Modification: an Effective Way of Avoiding the Collapse of SWNTs on Al Surface Revealed by Molecular Dynamics Simulations. Journal of Physical Chemistry C, 2009, 113, 14747-14752.	3.1	20
218	The Core/Shell Composite Nanowires Produced by Self-Scrolling Carbon Nanotubes onto Copper Nanowires. ACS Nano, 2009, 3, 2235-2240.	14.6	78
219	Temperature dependence of the electrical properties of the carbon nanotube/polymer composites. EXPRESS Polymer Letters, 2009, 3, 769-777.	2.1	85
220	Effect of chemisorption on the interfacial bonding characteristics of carbon nanotube–polymer composites. Polymer, 2008, 49, 800-808.	3.8	96
221	Abnormal current–voltage characteristics and metal–insulator transition of amorphous Fe-doped carbon films on Si substrates. Physica B: Condensed Matter, 2008, 403, 3434-3438.	2.7	0
222	Large dielectric constant of the chemically purified carbon nanotube/polymer composites. Materials Letters, 2008, 62, 4229-4231.	2.6	82
223	Influence of Nanotube Chirality, Temperature, and Chemical Modification on the Interfacial Bonding between Carbon Nanotubes and Polyphenylacetylene. Journal of Physical Chemistry C, 2008, 112, 16514-16520.	3.1	45
224	Controlled growth of hierarchical ZnO nanorods with periodical structure under negative feedback mechanism. Journal Physics D: Applied Physics, 2008, 41, 195402.	2.8	4
225	Forward tunneling effect and metal-insulator transition in the BaTiO3 film/Si n-n heterojunction. Applied Physics Letters, 2007, 91, 212105.	3.3	13
226	Ammonia sensitivity of amorphous carbon film/silicon heterojunctions. Applied Physics Letters, 2007, 91, .	3.3	35
227	The interface effect of the effective electrical conductivity of carbon nanotube composites. Nanotechnology, 2007, 18, 255705.	2.6	89
228	Abnormal current–voltage characteristics and metal–insulator transition of amorphous carbon film/silicon heterojunction. Physics Letters, Section A: General, Atomic and Solid State Physics, 2007, 371, 318-321.	2.1	7
229	Investigation of Molecular Interactions between SWNT and Polyethylene/Polypropylene/Polystyrene/Polyaniline Molecules. Journal of Physical Chemistry C, 2007, 111, 4628-4635.	3.1	176
230	Model for the effective thermal conductivity of carbon nanotube composites. Nanotechnology, 2006, 17, 1655-1660.	2.6	155
231	Study of giant magnetoresistance and giant electroresistance of carbon based thin film. Rare Metals, 2006, 25, 617-620.	7.1	4
232	Anomalous current–voltage characteristics and colossal electroresistance of amorphous carbon film on Si substrate. Applied Physics Letters, 2004, 85, 4397.	3.3	16
233	Effective dielectric constant of composite with interfacial shells. Physica B: Condensed Matter, 2004, 344, 129-132.	2.7	19
234	The influence of particle shape and size on electric conductivity of metal–polymer composites. European Polymer Journal, 2004, 40, 323-327.	5.4	129

#	Article	IF	CITATIONS
235	Anomalous positive magnetoresistance in Cox–C1â^'x granular films on Si substrates. Journal of Applied Physics, 2004, 95, 1906-1910.	2.5	24
236	A percolation model of metal–insulator composites. Physica B: Condensed Matter, 2003, 325, 195-198.	2.7	20
237	A NOVEL MODEL OF DIELECTRIC CONSTANT OF TWO-PHASE COMPOSITES WITH INTERFACIAL SHELLS. International Journal of Modern Physics B, 2002, 16, 3855-3863.	2.0	7
238	Giant magnetoresistance effect in Co–C bulk composites. Journal of Magnetism and Magnetic Materials, 2002, 246, 379-381.	2.3	7
239	Study on dielectric properties of oil/water random composites. Journal of Electrostatics, 2001, 50, 169-175.	1.9	8